AFRL-SR-AR-TR-10-0018

REPORT DOCUMENTATION PAGE

PLEASE DO NOT RETURN YOUR FORM TO THE ABOVE ORGANIZATION.

1. REPORT DATE *(DD-MM-YYYY)*	2. REPORT TYPE	3. DATES COVERED *(From - To)*
27-02-2010	Final Technical Report	1/12/2008 - 30/11/2009

4. TITLE AND SUBTITLE
GUIDING NEURONAL GROWTH IN TISSUES WITH LIGHT

5a. CONTRACT NUMBER
N/A

5b. GRANT NUMBER
FA9550-07-1-0130

5c. PROGRAM ELEMENT NUMBER

6. AUTHOR(S)
Dr. Jeffrey Urbach

5d. PROJECT NUMBER

5e. TASK NUMBER

5f. WORK UNIT NUMBER

7. PERFORMING ORGANIZATION NAME(S) AND ADDRESS(ES)
Georgetown University
37th and O Streets, NW
Washington, DC 20057

8. PERFORMING ORGANIZATION REPORT NUMBER

9. SPONSORING/MONITORING AGENCY NAME(S) AND ADDRESS(ES)
Air Force Office of Scientific Research
875 N. Randolph Street, Rm 3112
Arlington, VA 22203

NL

10. SPONSOR/MONITOR'S ACRONYM(S)

11. SPONSOR/MONITOR'S REPORT NUMBER(S)

12. DISTRIBUTION/AVAILABILITY STATEMENT
Approved for public release; distribution is unlimited.

13. SUPPLEMENTARY NOTES

20100427015

14. ABSTRACT

15. SUBJECT TERMS

16. SECURITY CLASSIFICATION OF:			17. LIMITATION OF ABSTRACT	18. NUMBER OF PAGES	19a. NAME OF RESPONSIBLE PERSON
a. REPORT	b. ABSTRACT	c. THIS PAGE			Jeff Urbach
U	U	U	UU	2	19b. TELEPHONE NUMBER *(Include area code)* 202-687-6594

Guiding Neuronal Growth in Tissues with Light

PI: Jeffrey S. Urbach
Institution: Georgetown University
Award FA9550-07-1-0130

Accomplishments:

Axonal Light Guidance:

Control over axonal trajectories is a critical component of engineering nerve regeneration and reconnection after injury and is essential for engineering specific connections in *in vitro* neural networks. .Neuronal networks interfaced with microelectrode arrays represent a promising class of cell-based biosensors because of their sensitivity to a broad range of neuroactive and toxic substances, but no satisfactory techniques exist for engineering interconnections between neurons or patterning neurons on sensing sites. A variety of approaches have been employed to guide extending axons but almost all have been employed on two dimensional or nearly two dimensional environments. Evidence from a wide range of systems shows that cells are sensitive to the mechanical and structural properties of their surroundings in addition to the biochemical properties. Furthermore, three-dimensional biopolymer matrices provide structural and physiological support that more closely mimics the *in vivo* environment and would allow for more complex network topologies.

It has recently been shown that weak optical forces, generated by an infrared laser spot placed adjacent to the leading edge of the growth cone of an extending axon, enhance growth into the beam focus and result in guided neurite turns, as well as enhanced. The mechanism through which the light modulates the direction of outgrowth is not known, but there is some evidence that the optical forces on the filopodia play an important role.

We investigated the viability of optical neurite guidance in three-dimensions. We analyzed the trajectories of neurites from differentiated PC12 cells cultured in a 3D matrix of collagen both with and without optical guidance. PC12 cells are often used as a model system for neural differentiation, and for examining growth cone behavior.

Approach: A 1064 nm Ytterbium fiber ring laser with collimated output was used as the light source for the optical beam. The laser beam passed through a neutral density filter to attenuate the laser output power. Power outputs ranged between 40-100 mW. The position of the laser beam in the focal plane was directed by a fast steering-mirror located at a plane optically conjugate to the rear aperture of the objective.

Throughout the optical guidance trials, the laser beam was repositioned frequently so that the beam spot remained near the leading edge of the extending neurite. The laser beam could be rapidly repositioned in the x and y directions with an accuracy of approximately 0.1 μm in the sample plane, allowing for precise oscillations of the laser position. At the beginning of a guidance trial, an intended trajectory was chosen, 90° from the current neurite direction. The focus of the beam was positioned on the part of the leading edge that was closest to the intended direction of guidance. The laser beam was placed over the leading edge of the growth cone so that about half of the beam was on top of the leading edge, and was oscillated at the leading edge of the growth cone at a rate of 0.1 Hz. The slow oscillation of the beam simulated a large beam size to make the optical trap more effective. The beam was oscillated with an amplitude of 1-2 microns, in

the direction that covered the most area of the growth cone possible and as many filopodia as possible. If the growth cone moved significantly out of the focal plane, the microscope was refocused to obtain a sharp image.

Findings: Prior to conducting the guidance trials, control trials were conducted to observe the typical frequency with which neurites changed their trajectory spontaneously. For each control trial, an isolated growth cone at least 30 μm from the coverslip was identified by visual inspection. The neuronal extension was imaged for a 10-minute trial period. If filopodial movement was apparent, or the cell advanced at least 1-2 μm in 10 minutes, the growth cone was presumed to be active. Only active growth cones were included for either control or optically guided trials. The growth cone was then imaged for an additional 30 minutes to observe the change in neurite trajectory over time. In all but one trial, the neurite extensions continued to grow approximately straight.

By contrast, eight out of ten optically guided trials displayed large changes in direction over the course of the experiment. The large changes in neurite trajectory may be observed clearly in the summary of the optically guided trials shown in Fig. 1.

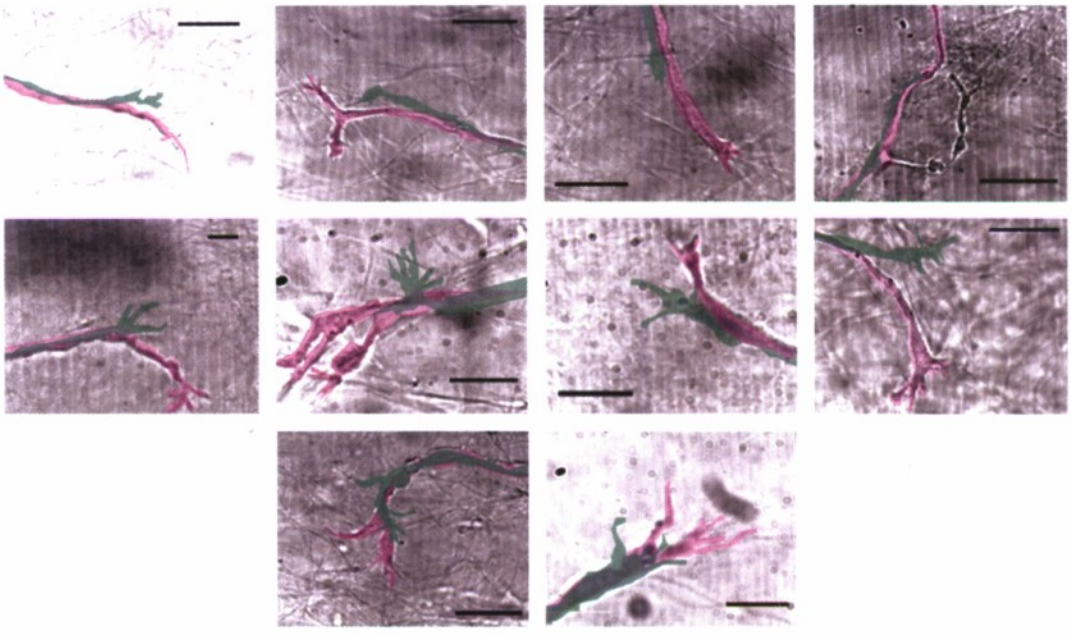

Fig. 1: Summary of Optically Guided Turns. The neurite at the beginning of the imaging period is shown in green, and the magenta overlays show the position at the end of the 30-40 minute trial. At the top are the eight successful trials, which clearly exhibit a change in neurite direction. The bottom two trials did not show significant turning: one of these failed guided trials seemed attracted and/or attached to several collagen fibrils in an direction different from the intended direction, while the other failed guided trial did not produce significant advance. (Scale bar: 10 μm)

In order to quantify the extent of turning, a change in angle was calculated for each trajectory. For the control trials, 9 of the 10 trajectories showed deviations of less than 5°. Eight out of ten guidance trials experienced large changes in orientation, always in the intended direction. Two trials experienced no or very little change in direction. The change in the neurite trajectory for the eight successful guided trials was about 52 ± 8 degrees (average ± SEM). These results are summarized in Fig. 2

The growth rate over the course of the imaging time was observed to be quite different between the controls and the guided trials. In the controls, the neurites advanced at an average rate of 0.37 ± 0.06 μm/minute, while the guided neurites advanced an average of 0.74 ± 0.1 μm/minute. This result shows that optical neuronal guidance in 3D substantially increases the rate of neurite outgrowth.

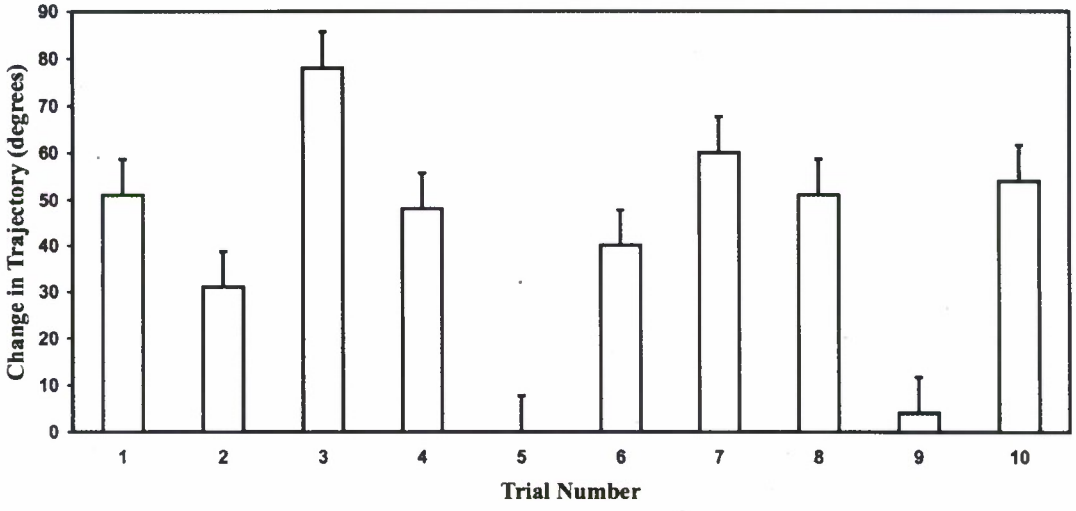

Fig. 2: Table of results for the change in neurite trajectory of guided trials. Eight of the ten trials showed a change in trajectory well above 5°. For the control trials, nine out ten trials showed changes in direction of less than 5°.

These results demonstrate quantitatively that light guidance is at least as effective in 3D gels than on 2D surfaces, opening up a wide range of potential applications for therapeutic interventions and biosensor development. This work was published in the Journal of Neuroscience Methods (full citation at end of report).

Intracellular Dynamics of Axon Guidance

We also performed studies of changes in cytoskeletal dynamics induced by external signals and developed innovative tools for measuring the mechanical interaction between axons and their environment. These studies provide the basis for optimizing guidance strategies for specific engineering contexts, and for developing artificial matrices that maximize the efficacy of light guidance.

Growing axons respond to positive and negative guidance cues, both soluble and substrate-bound, when navigating to their targets. This response is coordinated by the growth cone, but the mechanisms by which growth cones steer axons in response to guidance cues is not clear. We evaluated the effects on localized microtubule polymerization of both positive (NGF) and negative (CSPG) guidance cues in PC12 cells. NGF, in addition to its roles in survival and differentiation, serves as a strong positive guidance cue, while CSPGs provide repulsive guidance cues to developing and regenerating axons. Our results show that NGF and CSPGs have opposite effects on microtubule polymerization, increasing and decreasing the rate of microtubule polymerization, respectively. Significantly, the effect of CSPGs on microtubule

polymerization rate was localized to the neurites in direct contact with CSPGs; other neurites of the same cell were unaffected.

Approach: PC12 cells were transfected with GFP-EB3, allowing for visualization of polymerizing microtubules through live cell fluorescence imaging. Time-lapse images were obtained at 0.8 sec intervals, and custom tracking software was developed to quantify rates of microtubule polymerization. Boundaries were created on poly-L-lysine (PLL)-coated glass-bottomed dishes by adding spots of either CSPGs or HBSS (as a control). Polymerization rates were calculated for neurites in contact with spots, and compared with rates measured in neurites away from the spots.

Findings: We first compared the rates of microtubule polymerization in the presence and absence of NGF. NGF application promotes neurite formation in PC12 cells. Quantitative analyses of GFP-EB3 comets in 25 NGF-treated and 24 untreated PC12 cells indicated that NGF-treatment significantly increases microtubule polymerization rates. In untreated, NGF-naïve samples, the average microtubule polymerization rates were 13.4 ± 0.1 μm/min versus 16.2 ± 0.2 μm/min for cell bodies of NGF-treated cells. It has been reported that microtubule polymerization in neurites occurs both in the anterograde (away from the cell body) and the retrograde (towards the cell body) directions. We therefore examined the direction of trajectories in the cell bodies and the neurites. We found that the direction of microtubule polymerization is random in the cell bodies, while the microtubules in the neurites are primarily polymerizing toward the leading edge of the neurites .

In order to determine the effects of immobilized CSPGs on microtubule polymerization, live cell imaging was conducted on GFP-EB3 transfected PC12 cells whose neurites encountered CSPG- and HBSS-coated regions (Figure 3). As previously shown in neurons, the neurites crossed into the HBSS-coated regions (Figure 3A), but did not cross the interface with CSPGs (Figure 3B). We analyzed the rates of microtubule polymerization in three regions of the PC12 cells: cell bodies, neurites away from the interface, and neurites contacting the interface (Figure 3). We analyzed tracks from 18 NGF-treated cells at CSPG spots, and 24 cells at HBSS spots. As observed in NGF-treated cells, the microtubule polymerization rates were significantly slower in the neurites compared to cell bodies ($p < 0.05$). We compared the polymerization rates in neurites that were in direct contact with spots with rates in neurites that did not. We observed that contact with CSPGs had a significant effect on microtubule polymerization rate only in the neurites that were in direct contact with the proteoglycan (Figure 3C): we observed a reduction in median rate of microtuble polymerization of 16.0 μm/min in the cell body to 12.4 μm/min in the neurites at the spot ($p < 0.001$), while the median rate in the neurites away from the spot was 15.0 μm/min. On the other hand, there were no differences in microtubule polymerization rates of neurites that were in direct contact with HBSS-coated regions compared to those away from the HBSS. Thus, contact with CSPGs has a highly localized action on microtubule polymerization. Cumulative frequency histograms of the microtubule polymerization rates (Figure 3D, E) showed that the distributions overlap in the regions where cells are not in contact with CSPGs. At CSPG interfaces, however, there is a significant leftward shift in the distribution of comet

velocities, resulting in a large increase in the percentage of slow moving comets with a concomitant and significant decrease in the percentage of fast moving comets ($p < 0.01$). Taken together, these results strengthen our conclusion that CSPG boundaries alter microtubule dynamics via localized decreases in microtubule polymerization rates.

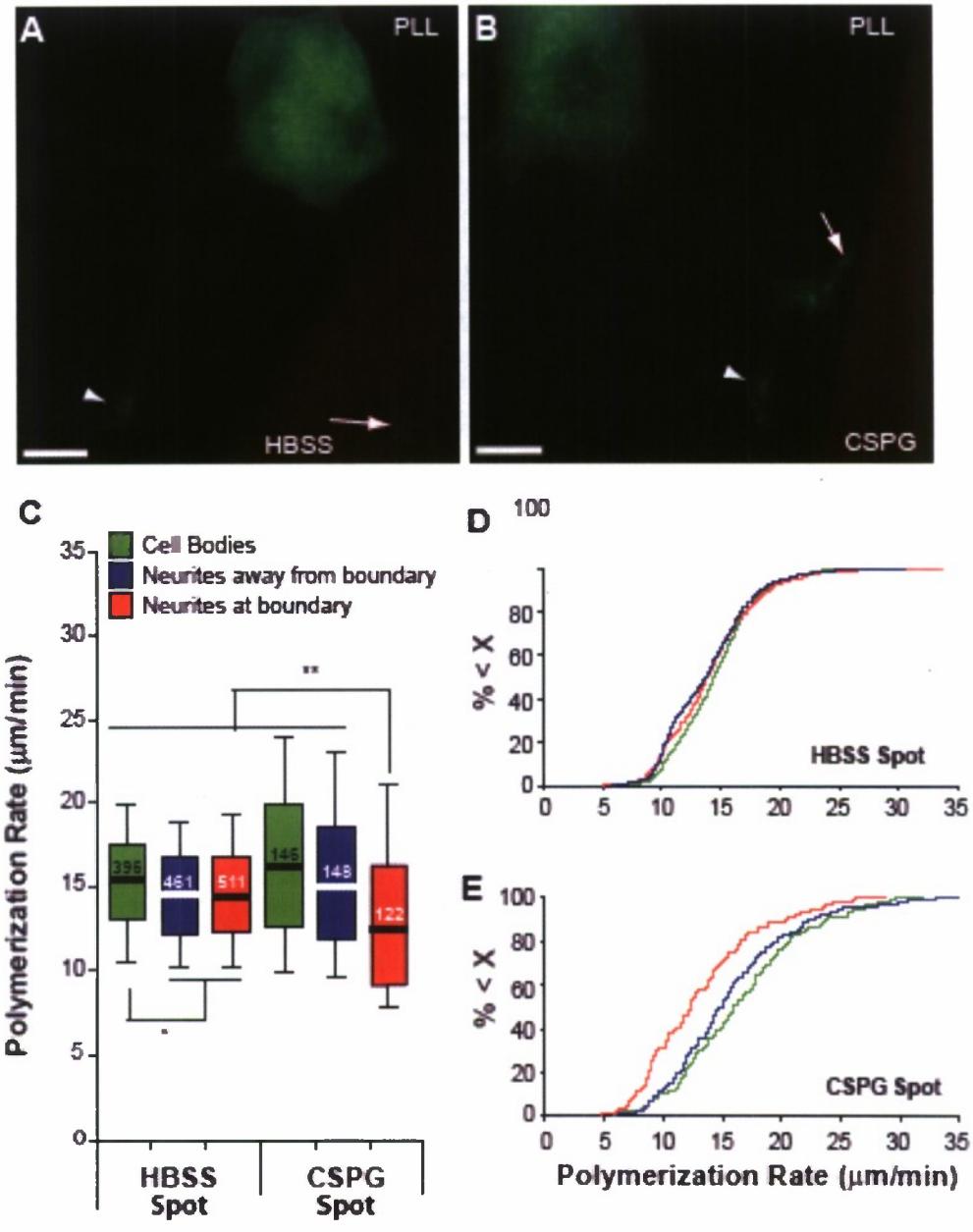

Fig. 3: Chondroitin sulfate proteoglycans (CSPG) create a boundary that produced significant localized reductions in microtubule polymerization rate. **A.** Control (HBSS) region does not create a boundary, i.e. neurites are able to cross into the region. **B.** CSPG regions create a boundary that prevent neurite crossing. For analysis, comet trajectories are localized in three distinct regions, the cell bodies, neurites away from the spot, and

neurites that are at or on spots (arrows). Scale bars are 10 μm. **C.** Box and whisker plots showing that microtubule polymerization rate is significantly reduced in neurites encountering CSPG spots (n = number of trajectories as indicated in figure, * $p < 0.05$ versus the cell bodies in HBSS encountering cells, ** $p < 0.001$ versus cell bodies and neurites away from the CSPG spots). Boxes are the upper and lower quartiles, whiskers are the maximum and minimum values and center line is the median value. **D, E.** Cumulative frequency histograms of the rates of microtubule polymerization in the cell bodies and neurites away from and at HBSS spots (D) and cell bodies and neurites away from and at CSPG spots (E).

Previous research had shown that, while the majority of microtubules polymerized in the anterograde direction (towards the distal end of the neurite), 13-35% of the microtubules polymerized in the retrograde direction. These data were obtained on uniform surfaces where neurites were extending spontaneously. However, as the growth cones encounter the CSPG boundary, stalling or retraction may occur as the filopodia sample the environment before being directed away from less permissive regions. We examined the direction of microtubule polymerization in a subset of neurites at or away from CSPG interfaces. For each neurite, all the trajectories were classified manually as either anterograde (away from the cell soma), retrograde (towards the cell soma), or neither. An example of a typical growth cone with the directions of polymerization is presented in Fig. 4A. Fig. 4B presents an example of a control neurite, in which, microtubules polymerize overwhelmingly in the anterograde direction. This can be visualized with the use of kymograph analysis in Fig. 4D. When the percentage of microtubules polymerizing in the anterograde and retrograde direction were quantified (Figure 4F), we observed that in control neurites, 14 ± 2% of microtubules polymerized in the retrograde direction versus 81 ± 3% in the anterograde direction. In contrast, in neurites that contacted CSPGs, (Figure 4C), a significantly higher percentage of microtubules polymerized in the retrograde direction (Figure 4E). Here, 35 ± 3% of the microtubules were polymerizing in the retrograde compared to 64 ± 3% polymerizing in the anterograde direction ($p < 0.001$ as compared to control). We also examined the rate of polymerization in neurites in the anterograde and retrograde directions (Figure 4G). We found that contact with the CSPGs resulted in a slowing of polymerization: while the rates of polymerization in neurites at control boundaries were almost equal, there was a significant decrease at CSPG boundaries. At HBSS spots, the median polymerization rates were 14.9 μm/min in the anterograde direction and 14.4 in the retrograde direction, while at CSPG boundaries the respective rates were 14.0 and 13.0 ($p < 0.05$). Thus, contact with CSPGs locally alters both the direction and rate of microtubule polymerization.

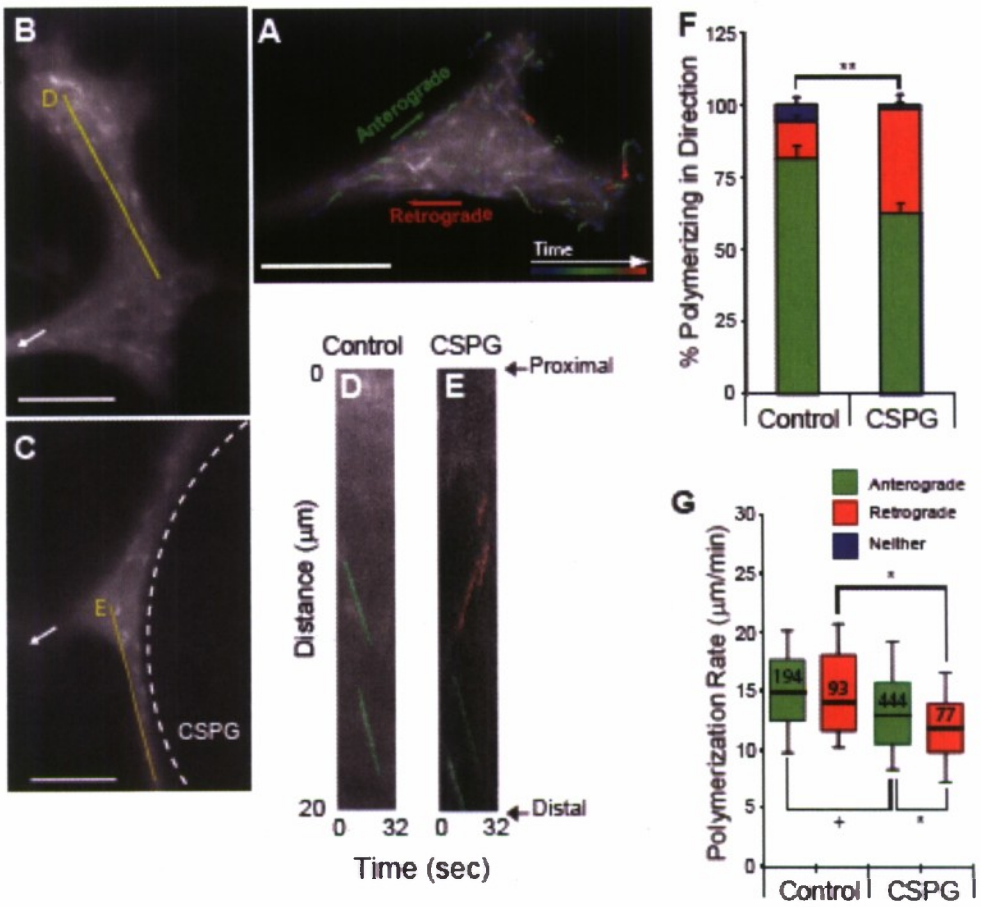

Fig. 4: Chondroitin sulfate proteoglycan (CSPG) spots significantly increase retrograde microtubule polymerization. **A.** Growth cone illustrating the classification of polymerization direction as either away from the cell body towards the leading edge (anterograde) or towards the neurite shaft and cell body (retrograde). **B.** Neurite that is not at spot. **C.** Neurite at CSPG spot. Arrows in B and C point towards the cell bodies. The dashed white line in C shows the location of the CSPG spot. Scale bars are 10 µm. **D.** Kymograph of the area outlined in the yellow box in B showing that in control cells the microtubule are polymerizing in the anterograde direction. Green dotted lines overlay anterograde trajectories. **E.** Kymograph of the area outlined in the yellow box in C showing that at CSPG spots there is an increase in the percentage of microtubules polymerizing in the retrograde direction. Green dotted lines overlay anterograde trajectories, while red lines overlay retrograde trajectories. **F.** Bars indicate the percentage of the microtubules polymerizing in either anterograde (green), retrograde (red) or neither (blue) direction. At CSPG boundaries, there is an increase in the percentage of microtubules polymerizing in the retrograde direction and a corresponding decrease in the percentage polymerizing in the anterograde direction ($n = 12 - 15$, ** $p < 0.001$). The data is presented as mean ± SEM. **G.** Box and whisker plots showing that the rate of microtubule polymerization was slower in the retrograde direction in neurites encountering CSPG-rich areas (n are the number of tracks as indicated in the figure, * $p < 0.05$, + $p < 0.01$). Boxes are the upper and lower quartiles, whiskers are the maximum and minimum values and center line is the median value.

These data suggest that local signaling and alterations in microtubule dynamic instability are essential features of growth cone response to guidance cues. Future studies will focus on identifying the receptors and the signal transduction pathways that control these processes, and mechanisms by which these processes can be manipulated to enhance control over axonal trajectories. This work was summarized in a manuscript currently under review at the Journal of Neuroscience Research.

Temporal Ordering from Fluorescence Correlation Analysis

As part of our research, we continued the development of novel tools for quantitative studies of intracellular dynamics using live cell imaging. We developed a technique using the temporal asymmetry of the cross-correlation function to determine the temporal ordering of spatially localized cellular events from multi-channel fluorescence imaging. Cell behaviors generally are triggered by specific combinations and temporal sequences of molecular signaling events. For instance, molecules can behave as switches: the association of an upstream protein to a receptor or signaling complex in turn triggers downstream proteins to associate. These pathways are typically complex, often with only weak and transient interactions between the components, and occur in an intrinsically noisy biochemical environment. Sorting out and understanding cellular pathways is one of the grand challenges of biology

Recent advances in live cell multi-channel fluorescence imaging has enabled the direct observation of spatial and temporal dynamics of cellular events. In practice, these observations are typically made by visual inspection, a process made problematic by subjective errors and biases, noise from the camera and background fluorescence, difficulty in obtaining quantitative information, and limitations to the amount of data that can be processed in this manner.

Correlation functions are a way to quantitatively aggregate information from noisy, stochastic time series; when applied to fluorescent movies, they operate directly on intensity values and do not require individual molecules or particles (e.g., speckles) to be resolved. We applied a fluorescence correlation approach that uses asymmetries in the temporal cross-correlation function to gain information about the temporal ordering in cellular reaction networks, building on the observation that temporal asymmetrics in correlation functions signify nonequilibrium processes.

The analysis is well suited to noisy, stochastic systems where the temporal order may not bc apparent in the raw data. The approach is applicable to any biochemical reaction not in chemical equilibrium, including protein complex assembly, sequential enzymatic processes, gene regulation, or other cellular signaling events. As an automated quantitative measure, it allows the data to be readily interpreted statistically with minimal subjective biases. We tested the technique using simulations of simple biophysical models with a definite temporal ordering, and then demonstrated the efficacy of the approach by extracting the temporal ordering of three proteins in the endocytic pathway: actin, sorting nexin 9, and clathrin. This work is described more fully in a manuscript that will be appearing shortly in the Biophysical Journal.

Mechanical Propcrties of Biopolymer Networks

Biopolymer networks exhibit unique nonlinear rheological behavior that differs dramatically from most synthetic materials. In particular, type I collagen fiber networks demonstrate substantial strain-stiffening and contractility over a broad range of concentrations. Type I collagen self-assembles in vitro to form percolated networks (gels) with mesh sizes ξ that depend on the concentration and polymerization conditions (Fig.

5A). These collagen networks are excellent model systems for investigating cellular motility in three-dimensional microenvironments, and provide bio-compatible scaffolds for tissue growth and organ regeneration. Unleashing the full potential of these applications requires an understanding of the connection between the nonlinear macroscopic rheology and the network microstructure. We investigated strain-stiffening of collagen networks under steady shear and found that the nonlinear rheology is strongly dependent on the material thickness. Moreover, the apparent moduli near yield decreases dramatically in thin samples in a process that is controlled by the ratio of the sample size to the network mesh size.

Approach: We apply continuous shear strains to collagen networks using a bulk rheometer with a parallel-plate geometry. The plate tool provides precise control of the sample thickness through a change of the rheometer gap h. We performed careful measurements of the stress σ on the gel as a function of the strain γ for a range of gaps. We also quantified the yield stress, σ_y, and yield strain, γ_y, as a measure of the ultimate strength of the gel. Images of the gel under shear were collected by an integrated confocal rheometer, allowing for direct observation of rearrangement events leading to strain stiffening.

Findings: At low strains, the measured stress is proportional to the applied strain for all values of h. Intermediate strains reveal that the network undergoes a substantial nonlinear increase of σ indicative of strain-stiffening. Higher strains lead to irreversible deformations and yielding as evidenced by a reduction in the overall modulus (Fig 5B). In addition to this distinctive rheological signature, we observed a dramatic change in the rheological response by varying the sample thickness from h = 50 - 300 μm, at a fixed collagen concentration. For gaps less than 200 μm, we found that the maximum of σ (γ) moves to larger values of γ (Fig. 5B). The yield strain in thin samples is more than twice that of thick samples, and the apparent modulus of thin samples can be up to 3 times smaller than the bulk value.

To quantify the h-dependence of the nonlinear rheology, used the peak positions to define the *yield* values for the stress σ_y and strain γ_y. We determined σ_y as a function of h for three different collagen concentrations. For each mesh size ξ (determined directly from confocal images), γ_y exhibits a clear increase for small h and approaches a constant value for large h (Fig. 5C). Interestingly, for the entire range of h the values of σ_y show weak or no gap dependence. We speculate that σ_y is determined by the strength of fiber-fiber or fiber-boundary junctions, and thus depends only on the total applied stress, independent of h.

Fig. 5D shows the data in Fig. 5C re-plotted with h rescaled by ξ. To account for the concentration dependent modulus, we also rescale σ_y by the ξ-dependent plateau values σ_p, determined by fitting $\sigma_y(h)$ to an exponential decay with an offset. The data from the three concentrations collapse onto a single curve. Confocal images of the network under increasing strain magnitude show a fiber bent and rotated about its attachment point (Insct, Fig 5D) reaching maximal extension, and torn along the shear direction. This alignment of the fibers is the likely origin of the strain stiffening, but a further work is necessary to connect the change in orientation with the observed gap dependence.

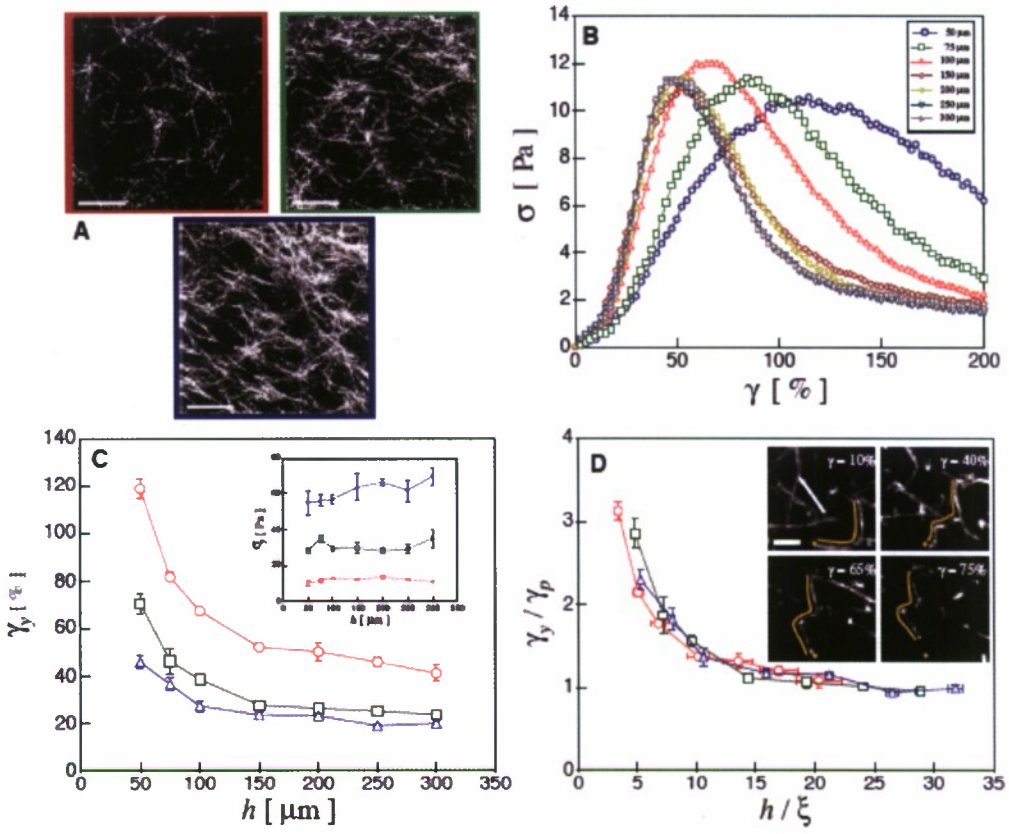

Fig 5: A. 10 μm maximum-projected confocal reflectance images of branched type I rat tail collagen fiber networks corresponding to 1 mg/ml (red), 2 mg/ml (green), and 3 mg/ml (blue) concentrations (scale bar = 25 _m). **B.** Stress-strain rheology curves for 1 mg/ml collagen gels at varying gaps h. (strain rate = 1% s^{-1}, error bars rcpresent standard error from four trials.) **C.** Yield strain versus gap for each collagen concentration extracted from rheology curves (B). (C inset) Yield stress σ_y versus h shows negligible gap dependence. **D.** Rescaling γ_y by the extrapolated plateau yield strain σ_p and h by ξ reduces (C) to a universal yielding curve. (D inset) Confocal rheology of magnified fluorescently-labeled branched fiber network at 2 mg/ml concentration under increasing strain magnitude in shear direction indicated by white arrow. Yellow line outlines fiber bent and rotated about its attachment point (yellow dot), reaching maximal extension, and torn along the shear direction (scale bar = 3 μm).

Note that the range of gaps investigated directly corresponds to the gap separation in many cone-plate tool geometries. An important implication of this result is that the nonlinear rheological response of collagen, and presumably other biopolymers, is not well defined in variable gap geometries. These findings have broad implications for the interpretation of rheological tissue data and the engineering of biomimetic scaffolds. These results are currently under review at Physical Review Letters.

Interactions:

We are continuing our collaboration with Dr. Herb Geller's group in NHLBI at the NIH to study axon motility in 3D biopolymer gels. We have shared cell culturing and transfection protocols, and they have incorporated some of the image analysis tools we have developed.

We are continuing our collaboration with the group of Jeff Gilman NIST to study the relationship between microstructure and rheology in nanocomposites. Using our unique imaging and image analysis capabilities, we are measuring the relationship between the structure of carbon nanotube networks and the elasticity and viscosity of the suspensions. We are also beginning a study of the properties of cellulose nanofiber suspensions.

We have initiated a collaboration with the Oxford silk group. Chris Holland has come to Georgetown twice to perform experiments with our confocal rheometer, and has been able to visualize, for the first time, shear induced silk fiber formation.

We are planning an exploratory project with David Kaplan's group at Tufts to investigate the structure and mechanical properties of the reversible silk e-gels that they have recently discovered.

Publications:

- C. Graves, R. McAllister, W. Rosoff, J. Urbach, "Optical neuronal guidance in three dimensional matrices", J. Neuroscience Meth **179**, 278 (2009).
- D.R.Sisan, D. Yarar, C. M. Waterman, J. S. Urbach, "Event ordering in live cell imaging determined from temporal cross correlation asymmetry", Biophysical Journal, in press.
- R. C. Arevalo, J. S. Urbach, and D. L. Blair, "Thickness-dependent rheology of collagen networks", submitted to Physical Review Letters.
- T.N. Kelly, I. Chen, P. Kumar, Y. Katagiri, K. Vartanian, E. Capuani, T. Thach, W. Rosoff, H. Wang, J. S, Urbach, H. Geller, "Localized alteration of microtubule polymerization in neurites that are in contact with chondroitin sulfate proteoglycans", submitted to Journal of Neuroscience Research.